Research Article

Advances in Mechanical Engineering

Advances in Mechanical Engineering
2017, Vol. 9(11) 1–12
© The Author(s) 2017
DOI: 10.1177/1687814017734513
journals.sagepub.com/home/ade
SAGE

Analysis and design of symmetric notch flexure hinges

Ning Xu[1,2], Ming Dai[1] and Xiaoqin Zhou[3]

Abstract

This article presents the analytic models of four types of flexure hinges (elliptic, circular, parabolic, and hyperbolic flexure hinges). The analytic models are developed based on the theory of elasticity and infinitesimal method. The hinge index, denoted by the ratio of rotational precision and rotational stiffness, is proposed in this article to estimate the mechanical properties of diverse flexure hinges synthetically and quantitatively. The finite element analysis method and the experiments are performed to verify the accuracy of the analytic model. The relationships between the geometric parameters and the mechanical properties of the flexure hinges are analyzed using the analytic models established in this article. The comparisons of the mechanical performances among the four types of flexure hinges are performed.

Keywords

Flexure hinge, stiffness, rotational precision, hinge index

Date received: 13 April 2017; accepted: 8 September 2017

Handling Editor: Davood Younesian

Introduction

The flexure hinge is a special mechanical component that produces the limited angular motion utilizing the micro-elastic deformation of the material, which possesses the advantages of no friction, zero backlash, high sensitivity, and so on.[1–5] Because the flexure hinges have many advantages in structure and engineering application, they are widely used in aerospace, manufacturing, optics, bioengineering, and many other fields.[6–10] The flexure hinges can be classified into elliptic, circular, parabolic, hyperbolic notch flexure hinges, and so on according to the notch shapes as illustrated in Figure 1.

Paros and Weisbord[11] proposed flexure hinge design issues as early as 1965. The authors deduced the equations (including precise and simplified equations) for calculating the stiffness of flexure hinges, based on the material mechanics theory and the idealized assumptions. Smith et al.[12] studied the elliptic flexure hinges and developed the compliance equations based on those proposed by Paros and Weisbord. Then, the accuracy of the equations was verified by finite element method and experiment. Ryu and Gweon[13] presented the error modeling of flexure hinges during machining based on computer-based method. Ryu et al.[14] proposed a mathematical equation to optimize the design of a flexure hinge stage. Lobontiu et al.[15–17] carried out a systematic and detailed study of various flexure hinges. They introduced the closed-form solutions for the corner-filleted flexure hinges and the conic-section flexure hinges based on Castigliano's second theorem. The finite element analysis (FEA) was applied to confirm the accuracy of the equations. Wu and Zhou[18] deduced the equations of general flexure hinges. The design equations were the results of accurate derivation and

[1]Changchun Institute of Optics, Fine Mechanics and Physics, Chinese Academy of Sciences, Changchun, China
[2]University of Chinese Academy of Sciences, Beijing, China
[3]School of Mechanical Science and Engineering, Jilin University, Changchun, China

Corresponding author:
Ning Xu, Changchun Institute of Optics, Fine Mechanics and Physics, Chinese Academy of Sciences, Changchun 130033, China.
Email: xuninghit@163.com

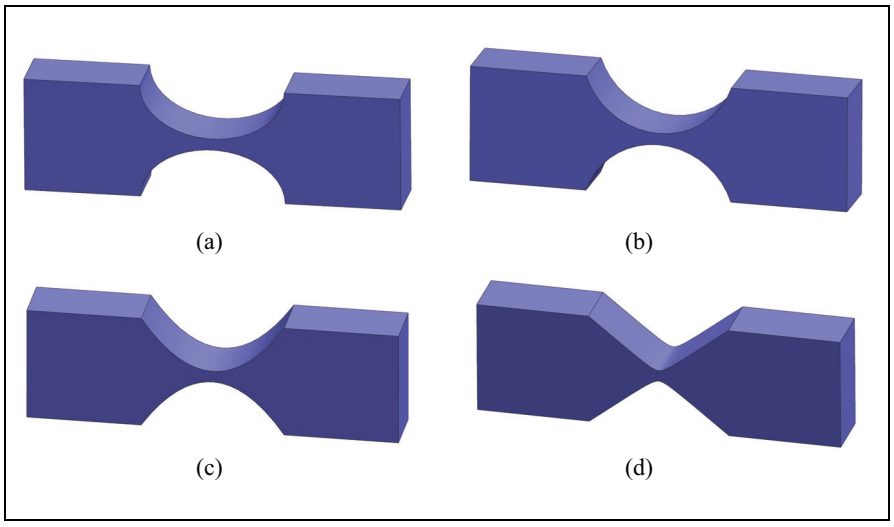

Figure 1. Four types of flexure hinges: (a) elliptic hinge, (b) circular hinge, (c) parabolic hinge, and (d) hyperbolic hinge.

were more concise in expression than those proposed by Paros and Weisbord. Tseytlin[19] presented effective equations for notch flexure hinges based on inverse conformal mapping method. The equation results were proved to be much more accurate than other theoretical equations. Yong et al.[20] presented the comparison of various stiffness equations of circular flexure hinges with the finite element results, and proposed more accurate empirical stiffness equations. Wang et al.[21] made a deep analysis and comparison of bow, straight beam, the corner-filleted, and compound type flexure hinges, and developed the relevant theoretical models of the usual flexure hinges. Qiu et al.[22] developed a multi-objective optimization mathematical model of flexure hinges with structural parameters as design variables and the right circular flexure hinges were optimized without considering the influence of the shear force. Yin et al.[23] established parameter optimization model for shallow notch elliptic flexure hinges, but only considered the role of effective torch. Lu et al.[24] established the stiffness model for the deep-notch elliptic flexure hinges and the deep-notch elliptic flexure hinges were optimized based on the model.

The stiffness and rotational precision of flexure hinges are the most crucial factors to be considered during the flexure hinges design. In order to accurately calculate the above parameters, this article develops analytic model for the characteristics of four types of flexure hinges (Figure 1), based on the theory of elasticity and infinitesimal method. The hinge index is proposed and defined to compare the performances of different flexure hinges quantitatively. To verify the accuracy of the analytic models, the FEA method and the experiments are performed for a large number of different dimensions of the flexure hinges. The errors between the results of the theoretical model calculations and FEA are less than 5%, and the ones between the theoretical and experimental are less than 6%. The mechanical properties of four kinds of flexure hinges are analyzed and compared with geometric parameters.

Analytic model of flexure hinges

The predecessors have done a lot of work on the establishment of analytic model of flexure hinges. But most of the models were based on the Euler–Bernoulli beam theory. The Euler–Bernoulli beam theory ignores the effect of shear deformation, so the results are not accurate. The theory of elasticity without plane assumption is the most accurate beam theory at present.

In this work, the theory of elasticity is used to calculate the stiffness and rotational precision of flexure hinges. Because the notch shapes of various flexure hinges are complicated, the notch is divided into numerous rectangle section unit beams to simplify the calculation. First, the displacements of the unit beam are solved; then, the sum of those displacements can be calculated for the displacements of the flexure hinges efficiently and precisely.

Displacements of rectangle cross-section unit beam

The rectangle section unit beam can be assimilated to a fixed-end flextensional element. The geometric parameters and loads are illustrated in Figure 2. Next, we can calculate the free-end axial displacement u, deflection v, and rotation angle α based on the theory of elasticity.

Assuming the stress function is $\Phi = Axy + By^2 + Cy^3 + Dxy^3$.

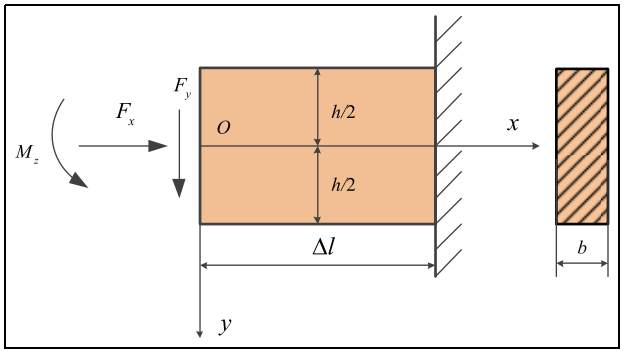

Figure 2. Geometric parameters and loads of rectangle section unit beam.

It meets the compatibility condition $(\partial^4\Phi/\partial x^4) + 2(\partial^4\Phi/\partial x^2\partial y^2) + (\partial^4\Phi/\partial y^4) = 0$.

Thus, the relevant stresses are

$$\begin{cases} \sigma_x = \dfrac{\partial^2\Phi}{\partial y^2} = 2B + 6Cy + 6Dxy \\ \sigma_y = \dfrac{\partial^2\Phi}{\partial x^2} = 0 \\ \tau_{xy} = -\dfrac{\partial^2\Phi}{\partial x\partial y} = -(A + 3Dy^2) \end{cases} \tag{1}$$

The following coefficients can be solved according to boundary constraints

$$A = \frac{3F_y}{2bh}, \quad B = -\frac{F_x}{2bh}, \quad C = -\frac{2M_z}{bh^3}, \quad D = -\frac{2F_y}{bh^3}$$

So, the specific stress expressions are

$$\begin{cases} \sigma_x = -\dfrac{F_x}{bh} - \dfrac{12M_z}{bh^3}y - \dfrac{12F_y}{bh^3}xy \\ \sigma_y = 0 \\ \tau_{xy} = \dfrac{3F_y}{2bh}\left(\dfrac{4}{h^2}y^2 - 1\right) \end{cases} \tag{2}$$

The related physical equations are

$$\begin{cases} \varepsilon_x = \dfrac{1}{E}(\sigma_x - \mu\sigma_y) \\ \varepsilon_y = \dfrac{1}{E}(\sigma_y - \mu\sigma_x) \\ \gamma_{xy} = \dfrac{2(1+\mu)}{E}\tau_{xy} \end{cases} \tag{3}$$

The relevant geometric equations are

$$\begin{cases} \dfrac{\partial u}{\partial x} = \varepsilon_x \\ \dfrac{\partial v}{\partial y} = \varepsilon_y \\ \dfrac{\partial v}{\partial x} + \dfrac{\partial u}{\partial y} = \gamma_{xy} \end{cases} \tag{4}$$

Combining equations (2)–(4) results in displacement components

$$\begin{cases} u = -\dfrac{12M_z}{Ebh^3}xy - \dfrac{6F_y}{Ebh^3}x^2y - \dfrac{F_x}{Ebh}x + \dfrac{2(2+\mu)F_y}{Ebh^3}y^3 + \omega y + u_0 \\ v = \dfrac{6\mu M_z}{Ebh^3}y^2 + \dfrac{6\mu F_y}{Ebh^3}xy^2 + \dfrac{\mu F_x}{Ebh}y + \dfrac{2F_y}{Ebh^3}x^3 + \dfrac{6M_z}{Ebh^3}x^2 \\ \quad -\dfrac{3(1+\mu)F_y}{Ebh}x - \omega x + v_0 \end{cases} \tag{5}$$

where the arbitrary constants (ω, u_0, and v_0) are rigid body displacements, which depend on the constraints. The relevant constraints are

$$(u)_{\substack{x=l\\y=0}} = 0, \ (v)_{\substack{x=\Delta l\\y=0}} = 0, \ \left(\frac{\partial v}{\partial x}\right)_{\substack{x=\Delta l\\y=0}} = 0$$

Then, the coefficients can be calculated

$$u_0 = \frac{F_x\Delta l}{Ebh}, \quad v_0 = \frac{4F_y\Delta l^3}{Ebh^3} + \frac{6M_z\Delta l^2}{Ebh^3},$$
$$\omega = \frac{6F_y\Delta l^2}{Ebh^3} + \frac{12M_z\Delta l}{Ebh^3} - \frac{3(1+\mu)F_y}{Ebh}$$

The above coefficients are substituted into equation (5), which yields the displacement components of the cantilever

$$\begin{cases} u = -\dfrac{12M_z}{Ebh^3}xy - \dfrac{6F_y}{Ebh^3}x^2y - \dfrac{F_x}{Ebh}x + \dfrac{2(2+\mu)F_y}{Ebh^3}y^3 \\ \quad + \left(\dfrac{6F_y\Delta l^2}{Ebh^3} + \dfrac{12M_z\Delta l}{Ebh^3} - \dfrac{3(1+\mu)F_y}{Ebh}\right)y + \dfrac{F_x\Delta l}{Ebh} \\ v = \dfrac{6\mu M_z}{Ebh^3}y^2 + \dfrac{6\mu F_y}{Ebh^3}xy^2 + \dfrac{\mu F_x}{Ebh}y + \dfrac{2F_y}{Ebh^3}x^3 + \dfrac{6M_z}{Ebh^3}x^2 \\ \quad -\left(\dfrac{6F_y\Delta l^2}{Ebh^3} + \dfrac{12M_z\Delta l}{Ebh^3}\right)x + \dfrac{4F_y\Delta l^3}{Ebh^3} + \dfrac{6M_z\Delta l^2}{Ebh^3} \end{cases} \tag{6}$$

Thus, the free-end axial displacement u, deflection v, and rotation α of the rectangle section unit beam can be obtained

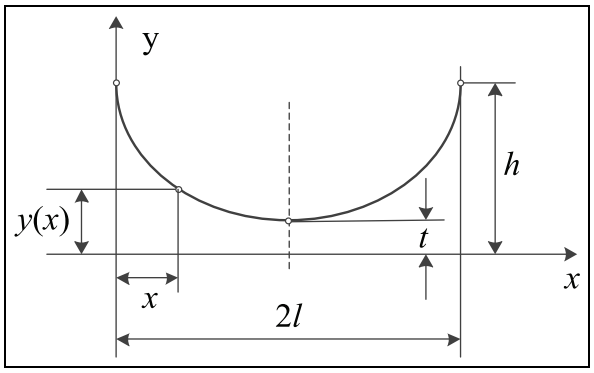

Figure 3. Parameters defining half of symmetric notch flexure hinge.

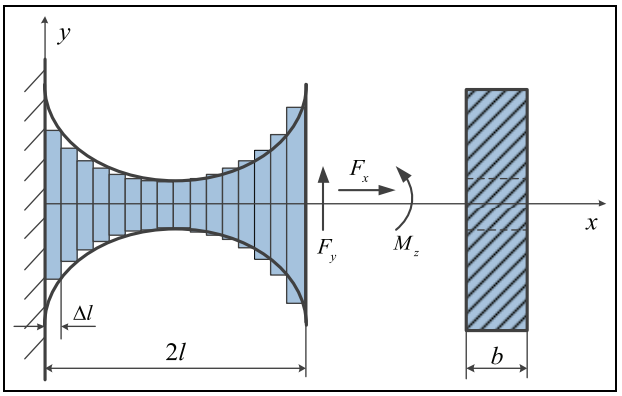

Figure 4. Unit division diagram of notch section.

$$\begin{cases} (u)_{\substack{x=0\\y=0}} = \dfrac{F_x \Delta l}{Ebh} \\ (v)_{\substack{x=0\\y=0}} = \dfrac{6M_z \Delta l^2}{Ebh^3} + \dfrac{4F_y \Delta l^3}{Ebh^3} \\ (\alpha)_{\substack{x=0\\y=0}} = \left(\dfrac{\partial v}{\partial x}\right)_{\substack{x=0\\y=0}} = -\left[\dfrac{12M_z \Delta l}{Ebh^3} + \dfrac{6F_y \Delta l^2}{Ebh^3}\right] \end{cases} \tag{7}$$

Displacements of flexure hinges

The flexure hinges consist of two cutouts that are symmetric with respect to both the longitudinal axis and the middle transverse one. The cross-section profile is curve of second order, specifically an ellipse, circle, parabola, and hyperbola. Now, we take the upper part of the symmetry flexure hinges to solve. The geometric parameters and coordinate axis are illustrated in Figure 3.

The variable thickness $t(x)$ can be expressed as:

(a) Elliptic flexure hinges

$$t(x) = 2y = 2\left[h - (h-t)\sqrt{1 - \left(\frac{x}{l-1}\right)^2}\right] \tag{8}$$

(b) Circular flexure hinges

$$t(x) = 2y = 2(R + t - \sqrt{R^2 - (x-l)^2}) \tag{9}$$

where $R = [(h-t)^2 + l^2]/2(h-t)$ is the radius of the circular notch.

(c) Parabolic flexure hinges

$$t(x) = 2y = 2\left[(h-t)\left(\frac{x}{l-1}\right)^2 + t\right] \tag{10}$$

(d) Hyperbolic flexure hinges

$$t(x) = 2y = 2t\sqrt{\left[\left(\frac{h}{t}\right)^2 - 1\right]\left(\frac{x}{l-1}\right)^2 + 1} \tag{11}$$

The notch section is divided into n rectangular section unit beams as shown in Figure 4. The length of every unit beam is $\Delta l = 2l/n$. Each element is considered as a separate rectangular section cantilever. Then, the displacement and rotation angle of the free end of each element are calculated. Finally, the displacements and rotation angles of all elements are summed. When the number of elements is sufficient, the total displacement and rotation angle are equal to those of the flexure hinge.

According to equation (7), the displacement and rotation of the first element are as follows

$$\begin{cases} u_1 = \dfrac{F_x \Delta l}{Ebt(\Delta l)} \\ v_1 = \dfrac{6[M_z + F_y(2l - \Delta l)]\Delta l^2}{Ebt^3(\Delta l)} + \dfrac{4F_y \Delta l^3}{Ebt^3(\Delta l)} \\ \alpha_1 = \dfrac{12[M_z + F_y(2l - \Delta l)]\Delta l}{Ebt^3(\Delta l)} + \dfrac{6F_y \Delta l^2}{Ebt^3(\Delta l)} \end{cases} \tag{12}$$

Define

$$\begin{cases} v'_1 = v_1 \\ \alpha'_1 = \alpha_1 \end{cases} \tag{13}$$

For the nth element

$$\begin{cases} u_n = \dfrac{F_x \Delta l}{Ebt(n\Delta l)} \\ v_n = \dfrac{6[M_z + F_y(2l - n\Delta l)]\Delta l^2}{Ebt^3(n\Delta l)} + \dfrac{4F_y \Delta l^3}{Ebt^3(n\Delta l)} \\ \alpha_n = \dfrac{12[M_z + F_y(2l - n\Delta l)]\Delta l}{Ebt^3(n\Delta l)} + \dfrac{6F_y \Delta l^2}{Ebt^3(n\Delta l)} \end{cases} \tag{14}$$

$$\begin{cases} v'_n = \Delta l \cdot \alpha'_{n-1} + v_n \\ \alpha'_n = \alpha'_{n-1} + \alpha_n \end{cases} \quad (15)$$

After above calculation, the displacement and rotation angle of flexure hinges under external loads are

$$\begin{cases} u = u_1 + u_2 + \cdots + u_n \\ v = v'_1 + v'_2 + \cdots + v'_n \\ \alpha = \alpha'_n \end{cases} \quad (16)$$

Stiffness

In high-precision instruments and equipment, the translation stiffness (K_x, K_y) and bending stiffness (K_α) of the flexure hinges are essential. Then, the stiffness is calculated below.

Let $F_y = 0$ and $M_z = 0$, the axial displacement $\boldsymbol{u}$ is calculated. Then, $K_x = F_x/u$.

Let $F_x = 0$ and $M_z = 0$, the deflection $\boldsymbol{v}$ is calculated. Then, $K_y = F_y/v$.

Let $F_x = 0$ and $F_y = 0$, the rotation angle $\boldsymbol{\alpha}$ is calculated. Then, $K_\alpha = M_z/\alpha$.

Precision of rotation

One of the basic requirements of a flexure hinge is that its rotational center remains unchanged during motion, but the center will be offset due to the elastic deformation of the material. Therefore, we should pay more attention to the rotational precision of the flexure hinge when designing a flexure hinge. Obviously, the greater the translational stiffness of the flexure hinges, the smaller the offset of the rotational center relative to the original position, that is, the higher the precision of rotation. So the translational stiffness is employed to measure the rotational precision of flexure hinges indirectly. Thus, the precision of rotation (P) is defined as follows

$$P = \sqrt{K_x^2 + K_y^2} \quad (17)$$

Hinge index

Flexure hinges are mainly designed to transfer rotational motion. The flexure hinges design with high performance is supposed to have lower bending stiffness and higher translational stiffness, as well as higher precision of rotation. So, in order to estimate the mechanical properties of diverse flexure hinges synthetically and quantitatively, this article proposes the dimensionless hinge index (N) of flexure hinges as follows

$$N = \frac{P}{K_\alpha} \quad (18)$$

The greater the index N, the better the comprehensive performance of the flexure hinge.

Verification of the analytic model

The finite element method was employed to test analytic model of flexure hinges. The FEA software NX-NASTRAN was applied to calculate the stiffness of four types of flexure hinges with several configurations under static loading. The material constants were $\rho = 8300\,\mathrm{kg/m^3}$, $E = 130\,\mathrm{GPa}$, and $\mu = 0.35$. The finite element mesh, one of the flexure hinges, is shown in Figure 5.

The results of FEA and analytic model are shown in Table 1 for four types of flexure hinges.

Furthermore, the experimental method was carried out to validate the analytical model. Due to good processability, the circular flexure flexures of stainless steel were used as the experimental specimens. The material constants were $\rho = 7800\,\mathrm{kg/m^3}$, $E = 200\,\mathrm{GPa}$, and $\mu = 0.28$. The sample was clamped on the workbench through the fixture. The force applied to the specimen could be controlled by the adjustment, the value of which would be measured by the dynamometer. At the same time, the dial gauge was used to measure the displacement of the specimen accurately. The whole experimental arrangement and the specimens used in the experiment are shown in Figures 6 and 7, respectively.

The results of analytic model and experiments are shown in Table 2 for eight circular flexure hinges.

From the above two tables, we can see that the maximum error between the analytic model calculation results and the finite element simulation ones is 4.8%, and the maximum error between analytic and experimental ones is 5.2%. Therefore, the analytic model of

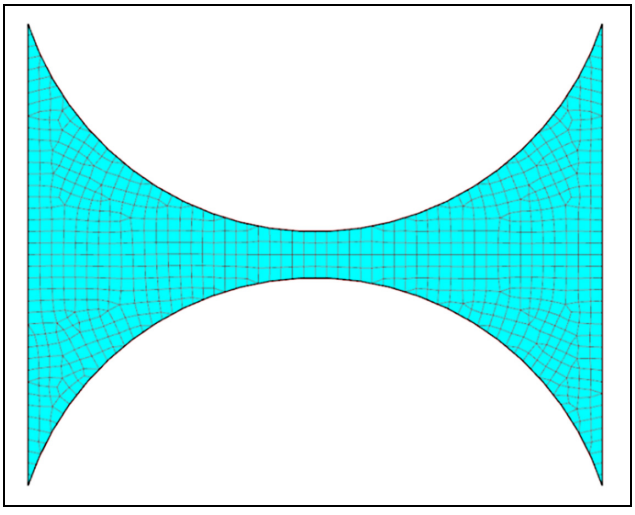

Figure 5. Finite element mesh of a flexure hinge.

Table 1. Analytical and finite element results for the stiffness.

	$2t$ (mm)	$2h$ (mm)	$2l$ (mm)	b (mm)	K_x (N/m)			K_y (N/m)			K_α (Nm/rad)		
					Analytical	FEA	Error (%)	Analytical	FEA	Error (%)	Analytical	FEA	Error (%)
Elliptic flexures	0.4	4	5	2	40.68	40.52	0.4	0.16	0.16	0	1.03	1.04	1.0
	0.4	4	5	4	81.37	82.17	1.0	0.31	0.32	3.1	2.06	2.11	2.4
	0.4	8	10	2	26.44	26.65	0.8	0.03	0.03	0	0.74	0.74	0.0
	0.4	8	10	4	52.88	53.65	1.4	0.06	0.06	0	1.47	1.53	3.9
	0.8	4	5	2	64.18	65.92	2.6	0.82	0.83	1.2	5.69	5.69	0
	0.8	4	5	4	128.37	129.89	1.2	1.64	1.62	1.2	11.38	11.33	0.4
	0.8	8	10	2	40.68	41.25	1.4	0.15	0.15	0	4.11	4.08	0.7
	0.8	8	10	4	81.37	82.24	1.1	0.31	0.31	0	8.22	8.25	0.4
Circular flexures	0.4	4	5	2	44.37	44.64	0.6	0.18	0.18	0	1.17	1.18	0.8
	0.4	4	5	4	88.73	87.34	1.6	0.36	0.36	0	2.34	2.40	2.5
	0.4	8	10	2	28.84	28.51	1.2	0.03	0.03	0	0.83	0.83	0
	0.4	8	10	4	57.70	57.44	0.5	0.06	0.06	0	1.65	1.69	2.4
	0.8	4	5	2	69.88	69.93	0.1	0.97	0.98	1.0	6.60	6.48	1.9
	0.8	4	5	4	139.68	138.81	0.6	1.94	1.87	3.7	13.20	12.95	1.9
	0.8	8	10	2	44.37	44.40	0.1	0.18	0.18	0	4.68	4.54	3.1
	0.8	8	10	4	88.73	89.45	0.8	0.36	0.35	2.9	9.35	9.33	0.2
Parabolic flexures	0.4	4	5	2	49.95	49.26	1.4	0.22	0.22	0	1.41	1.41	0
	0.4	4	5	4	99.90	99.70	0.2	0.44	0.44	0	2.83	2.95	4.1
	0.4	8	10	2	33.69	32.31	4.3	0.04	0.04	0	1.03	1.04	1.0
	0.4	8	10	4	67.39	65.15	3.4	0.08	0.08	0	2.05	2.06	0.5
	0.8	4	5	2	75.13	76.05	1.2	1.03	1.02	1.0	7.58	7.42	2.2
	0.8	4	5	4	150.29	148.61	1.1	2.13	2.12	0.5	15.17	14.95	1.5
	0.8	8	10	2	49.95	48.47	3.1	0.21	0.21	0	5.66	5.55	2.0
	0.8	8	10	4	99.90	97.66	2.3	0.44	0.43	2.3	11.31	11.29	0.2
Hyperbolic flexures	0.4	4	5	2	66.40	65.06	2.1	0.41	0.41	0	2.77	2.78	0.4
	0.4	4	5	4	138.29	140.53	1.6	0.87	0.84	3.6	5.55	5.47	1.5
	0.4	8	10	2	50.13	49.88	0.5	0.11	0.11	0	2.77	2.82	1.8
	0.4	8	10	4	112.65	108.99	3.4	0.22	0.21	4.8	5.55	5.37	3.4
	0.8	4	5	2	88.57	85.84	3.2	1.68	1.63	3.1	11.09	10.69	3.7
	0.8	4	5	4	177.81	174.92	1.7	3.35	3.27	2.4	22.19	22.23	0.2
	0.8	8	10	2	69.16	66.40	4.2	0.43	0.44	2.3	11.09	11.24	1.3
	0.8	8	10	4	138.29	135.28	2.2	0.87	0.89	2.2	22.19	21.32	4.1

Table 2. Analytical and experimental results for the circular flexure hinges.

No.	2t (mm)	2h (mm)	2l (mm)	b (mm)	K_x (N/m)			K_y (N/m)			K_α (Nm/rad)	
				Analytical	Experimental	Error (%)	Analytical	Experimental	Error (%)	Analytical	Experimental	Error (%)
1	0.4	4	5	2	68.24	65.90	3.6	0.27	0.27	0	1.80	1.85	2.7
2	0.4	4	5	4	136.48	143.44	4.9	0.55	0.56	1.8	3.60	3.52	2.3
3	0.4	8	10	2	44.38	46.22	4.0	0.05	0.05	0	1.27	1.32	3.8
4	0.4	8	10	4	88.75	87.48	1.5	0.10	0.10	0	2.54	2.51	1.2
5	0.8	4	5	2	107.48	110.92	3.1	1.48	1.43	3.5	10.16	9.88	2.8
6	0.8	4	5	4	214.97	226.79	5.2	2.97	2.91	2.0	20.31	19.86	2.3
7	0.8	8	10	2	68.24	69.78	2.2	0.27	0.28	3.6	7.19	7.27	1.1
8	0.8	8	10	4	136.48	143.57	5.0	0.55	0.54	1.9	14.39	14.36	0.2

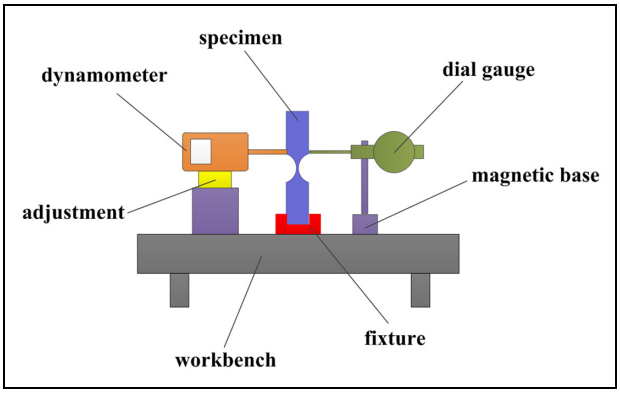

Figure 6. Layout of experiment.

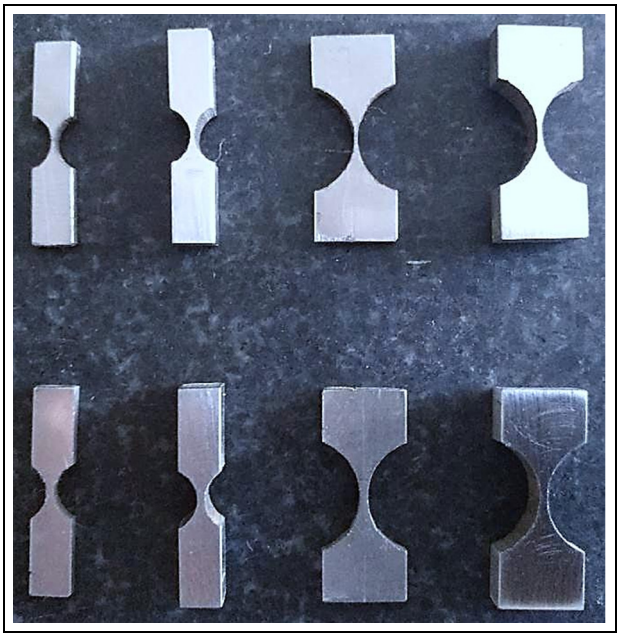

Figure 7. Specimens of circular flexure.

flexure hinges established in this article possesses high precision. The errors may come from the following factors: the meshing error, the manufacturing error, or the material property error. This model is then used to explore the relationships between the geometric parameters and mechanical properties of the flexure hinges.

Discussion

In the process of flexure hinges design, a clear understanding of the relationships between the geometric parameters and mechanical properties of flexure hinges will contribute to design a high-performance flexure hinge accurately and rapidly. The performance comparisons will indicate the direction of the flexure hinges design. When calculating the mechanical properties of

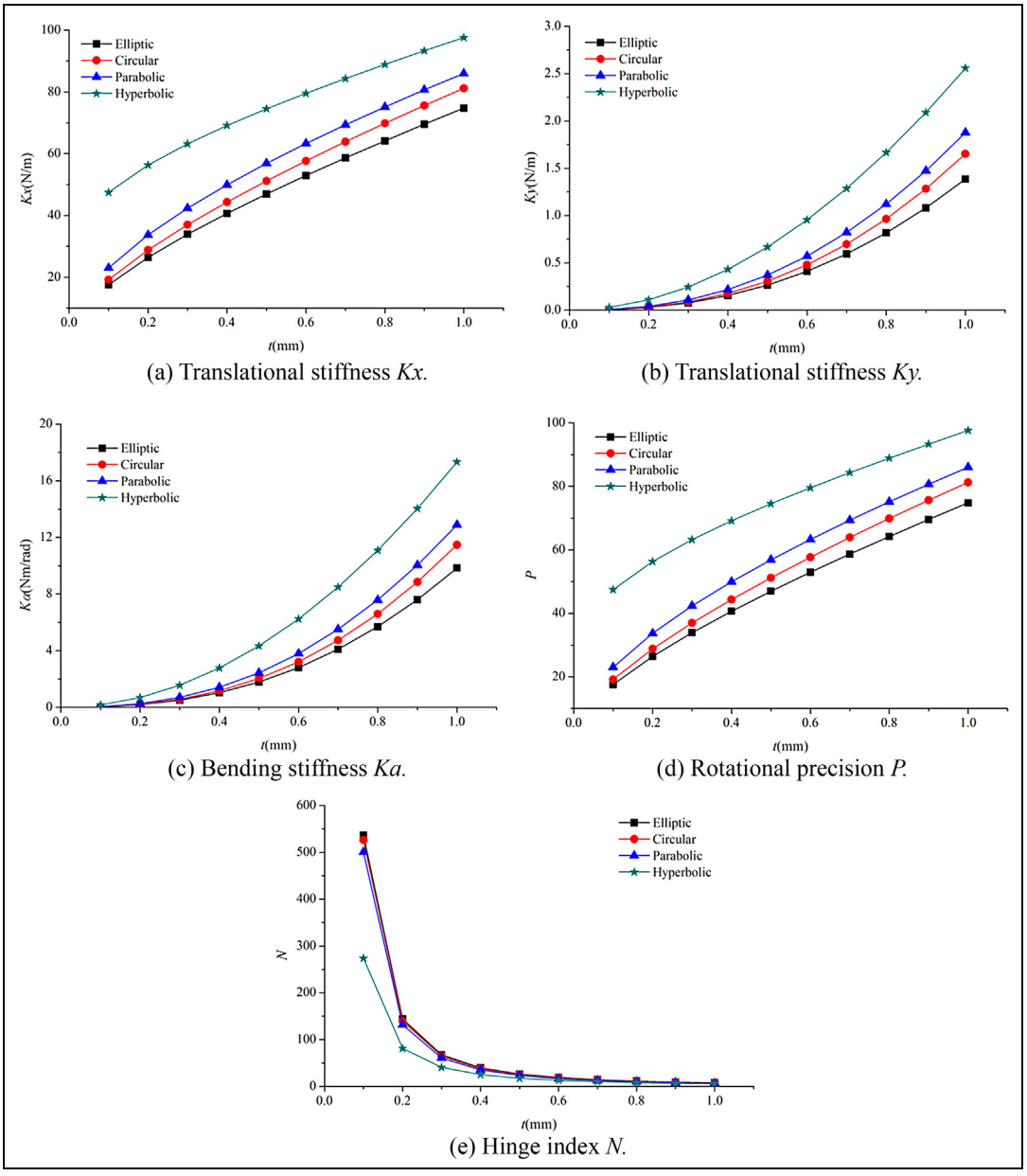

Figure 8. Comparisons of flexure hinges with minimum thickness *t*: (a) translational stiffness K_x, (b) translational stiffness K_y, (c) bending stiffness K_α, (d) rotational precision *P*, and (e) hinge index *N*.

flexure hinges, the material properties remain constant as described in section "Verification of the analytic model," but the minimum thickness t, the height h, the length l, and the depth b vary within a range for practical flexure hinges. Utilizing the established analytic model, the relative relationships of the mechanical characteristic parameters (K_x, K_y, K_α, P, and N) and the geometric parameters (t, h, l, and b) are calculated and organized into the following figures.

The comparisons of mechanical properties of the four types of flexure hinges with geometric parameter t are shown in Figure 8, where the minimum thickness t varies from 0.1 to 1.0 mm and the other geometric parameters remain unchanged. It can be seen from the figure that the stiffness (K_x, K_y, and K_α) and rotational precision (P) increase with the increasing minimum thickness t. The hinge index (N) decrease as t increases because K_α increases at rate much greater than that at which P increase with t increase as shown in Figure 8.

The comparisons of mechanical properties of four types of flexure hinges with h are shown in Figure 9, where the height h varies from 1.0 to 10.0 mm and the other geometric parameters remain unchanged. The figures show that the stiffness and rotational precision

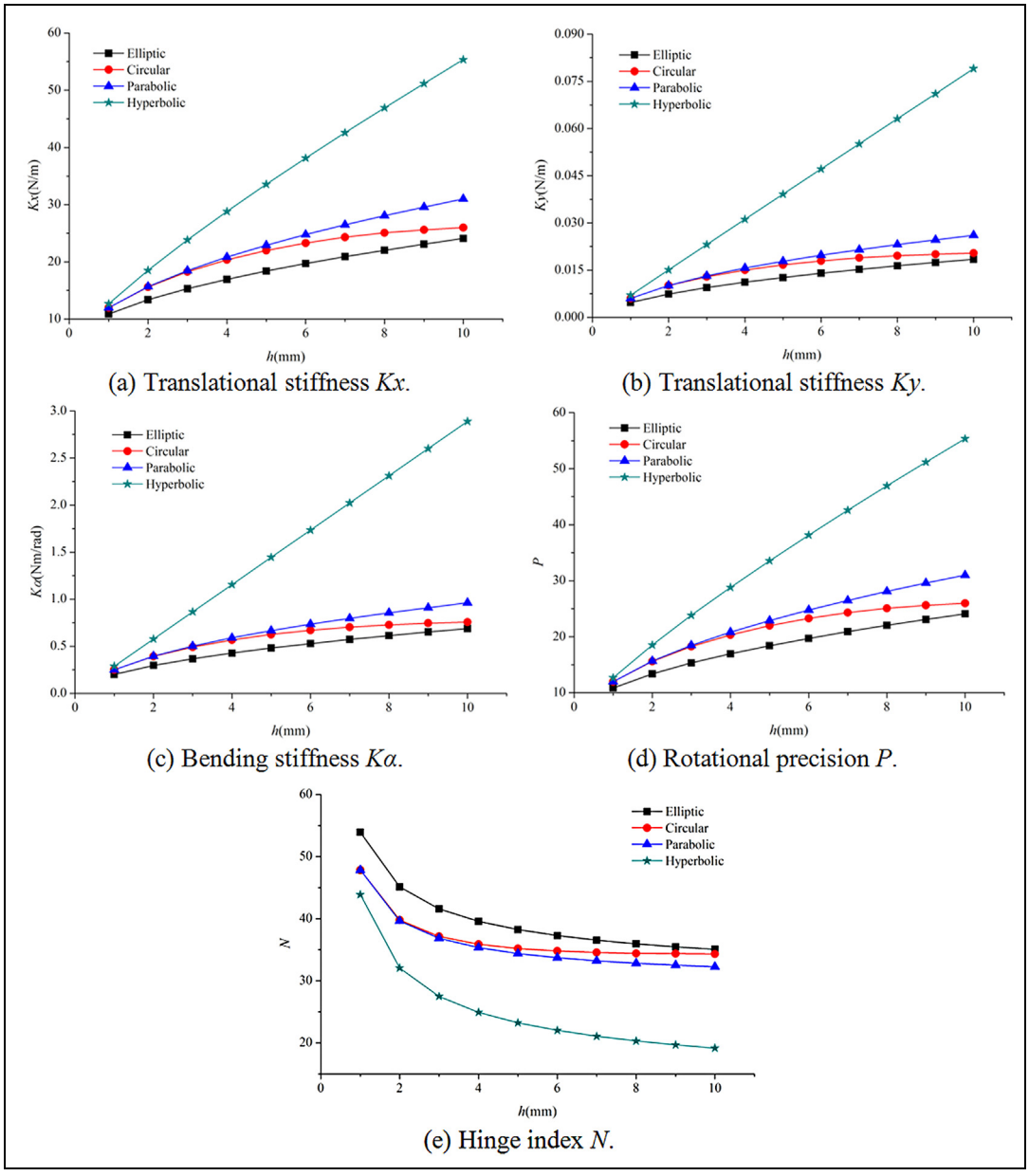

Figure 9. Comparisons of flexure hinges with the height h: (a) translational stiffness K_x, (b) translational stiffness K_y, (c) bending stiffness K_α, (d) rotational precision P, and (e) hinge index N.

increase, while the hinge index decreases with the increasing height h. The hinge index decreases for the same reason just as the effect of t on it. The circular flexure hinge performs like the parabolic one, but becomes more and more close to the elliptic one as h increases.

The comparisons of mechanical properties for four types of flexure hinges with l are shown in Figure 10, where the height l varies from 5.0 to 14.0 mm and the other geometric parameters remain unchanged. From the figures, we can see that the stiffness and rotational precision decrease with the increasing length. The hinge index remains almost constant as l grows. The circular flexure hinge performs like the elliptic one, but becomes more and more close to the parabolic one as l increases. This is exactly the opposite of h.

The comparisons of mechanical properties of four types of flexure hinges with b are shown in Figure 11, where the depth b varies from 1.0 to 5.5 mm and the other geometric parameters remain unchanged. The figures show that the stiffness and rotational precision increase with the increasing depth. And b has no effect on the hinge index.

From Figures 8–11, we can see that when all the geometric parameters are the same the order of

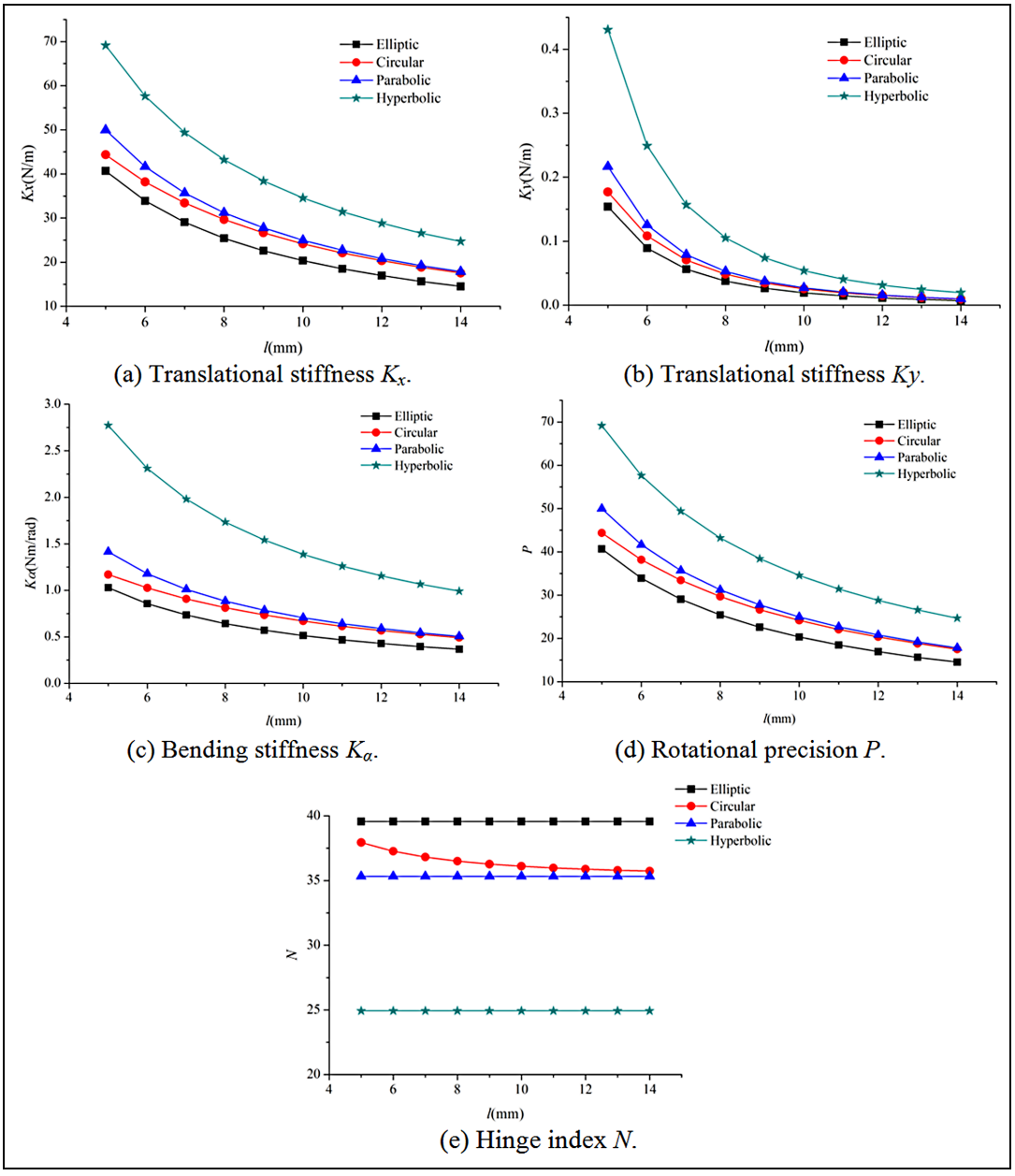

Figure 10. Comparisons of flexure hinges with the length l: (a) translational stiffness K_x, (b) translational stiffness K_y, (c) bending stiffness K_α, (d) rotational precision P, and (e) hinge index N.

compliance is elliptic, circular, parabolic, and hyperbolic flexure hinges; the order of rotational precision from high to low is hyperbolic, parabolic, circular, and elliptic flexure hinges; the order of hinge index from high to low is elliptic, circular, parabolic, and hyperbolic flexure hinge.

Conclusion

Based on the theory of elasticity, the analytic models for the elliptic, circular, parabolic, and hyperbolic flexure hinges have been established using the infinitesimal method. The expressions of the stiffness and rotational precision were provided, and the hinge index was proposed to evaluate the performance of flexure hinges. The research efforts were carried out to explore the relationships between geometric parameters and mechanical properties of flexure hinges.

The results showed that, for the four types of flexure hinges, the stiffness and rotational precision increase as geometric parameters t, h, and b increase, but decrease as l increases; the hinge index decreases as t and h increase, but remain constant as l and b change. For the same geometric parameters, the hyperbolic flexure hinges perform the highest rotational precision but the worst compliance, while the elliptic hinges perform

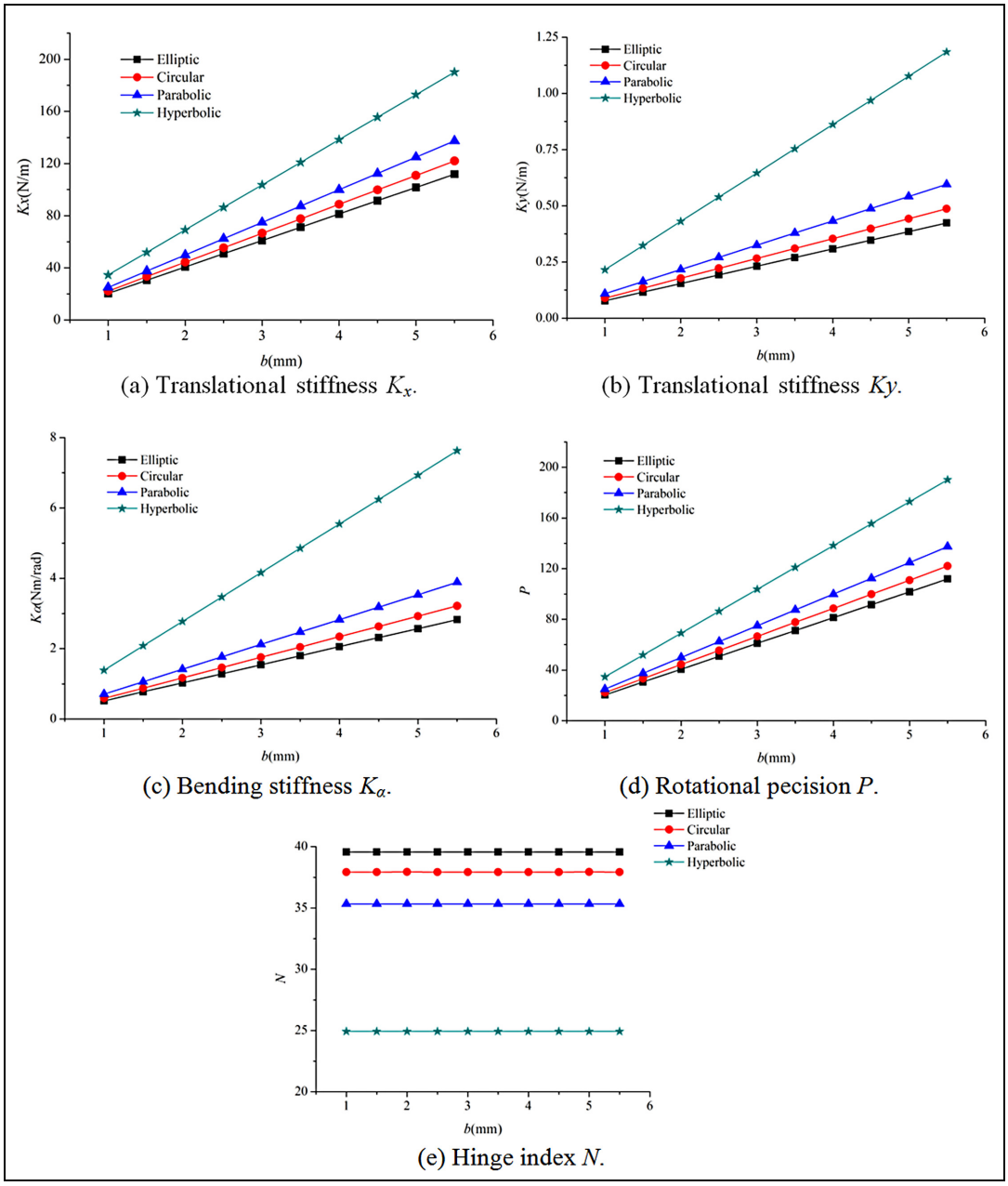

Figure 11. Comparisons of flexure hinges with the depth b: (a) translational stiffness K_x, (b) translational stiffness K_y, (c) bending stiffness K_α, (d) rotational precision P, and (e) hinge index N.

exactly the opposite. In the view of hinge index, the performance of the elliptic flexure hinges is better than that of the hyperbolic ones. The analytic model established by this article can provide theoretical guidance for the design of flexure hinges, which contribute to design flexure hinges with excellent performance.

Declaration of conflicting interests

The author(s) declared no potential conflicts of interest with respect to the research, authorship, and/or publication of this article.

Funding

The author(s) disclosed receipt of the following financial support for the research, authorship, and/or publication of this article: This work was supported by The Major Innovation Projects, Changchun Institute of Optics, Fine Mechanics and Physics, Chinese Academy of Sciences (Grant No. Y3CX1SS14C).

References

1. Tian Y, Shirinzadeh B and Zhang D. Design and dynamics of a 3-DOF flexure-based parallel mechanism

for micro/nano manipulation. *Microelectron Eng* 2010; 87: 230–241.
2. Kyoungchon K, Dahoon A and Daegab G. Optimal design of a 1-rotational DOF flexure joint for a 3-DOF H-type stage. *Mechatronics* 2012; 22: 24–32.
3. Yao Q, Dong J and Ferreira PM. Design, analysis, fabrication and testing of a parallel-kinematic micropositioning XY stage. *Int J Mach Tool Manu* 2007; 47: 946–961.
4. Liaw HC and Shirinzadeh B. Robust generalised impedance control of piezo-actuated flexure-based four-bar mechanisms for micro/nano manipulation. *Sensor Actuat A-Phys* 2008; 148: 443–453.
5. Alici G and Shirinzadeh B. Optimum dynamic balancing of planar parallel manipulators based on sensitivity analysis. *Mech Mach Theory* 2006; 41: 1520–1532.
6. Al-Kindi GA and Shrinzadeh B. An evaluation of surface roughness parameters measurement using vision-based data. *Int J Mach Tool Manu* 2007; 47: 697–708.
7. Liaw HC and Shirinzadeh B. Enhanced adaptive motion tracking control of piezo-actuated flexure-based four-bar mechanisms for micro/nano manipulation. *Sensor Actuat A-Phys* 2008; 147: 254–262.
8. Zhang D, Chetwynd DG, Liu X, et al. Investigation of a 3-DOF micro-positioning table for surface grinding. *Int J Mech Sci* 2006; 48: 1401–1408.
9. Liaw HC, Shirinzadeh B and Smith J. Robust motion tracking control of piezo-driven flexure-based four-bar mechanism for micro/nano manipulation. *Mechatronics* 2008; 18: 111–120.
10. Mohd Zubir MN and Shirinzadeh B. Development of a high precision flexure-based microgripper. *Precis Eng* 2009; 33: 362–370.
11. Paros JM and Weisbord L. How to design flexure hinges. *Mach Des* 1965; 37: 151–156.
12. Smith ST, Badami VG, Dale JS, et al. Elliptical flexure hinges. *Rev Sci Instrum* 1997; 68: 1474–1483.
13. Ryu JW and Gweon DG. Error analysis of a flexure hinge mechanism induced by machining imperfection. *Precis Eng* 1997; 21: 83–89.
14. Ryu JW, Gweon DG and Moon KS. Optimal design of a flexure hinge based XYθ wafer stage. *Precis Eng* 1997; 21: 18–28.
15. Lobontiu N, Paine JSN, Garcia E, et al. Corner-filleted flexure hinges. *J Mech Des-T ASME* 2001; 123: 346–352.
16. Lobontiu N, Paine JSN, Malley EO, et al. Parabolic and hyperbolic flexure hinges: flexibility, motion precision and stress characterization based on compliance closed-form equations. *Precis Eng* 2002; 26: 183–192.
17. Lobontiu N, Paine JSN, Garcia E, et al. Design of symmetric conic-section flexure hinges based on closed-form compliance equations. *Mech Mach Theory* 2002; 37: 477–498.
18. Wu YF and Zhou ZY. Design calculations for flexure hinges. *Rev Sci Instrum* 2002; 73: 3010–3016.
19. Tseytlin YM. Notch flexure hinges: an effective theory. *Rev Sci Instrum* 2002; 73: 3363–3368.
20. Yong YK, Lu TF and Handley DC. Review of circular flexure hinge design equations and derivation of empirical formulations. *Precis Eng* 2008; 32: 63–70.
21. Wang XS, Chen GP, Zhou JH, et al. Compliant mechanisms consisted of compound flexible hinges and its applications. *Opt Precis Eng* 2005; 13: 91–97.
22. Qiu LF, Nan TL and Weng HS. Multi-objective optimization for rotation capacity of flexure hinges. *J Univ Sci Technol B* 2008; 30: 189–192.
23. Yin WT, Rui YN and Li R. Fuzzy optimization of the elliptical flexure hinge in micro-gripper. *Mach Tool Hydraul* 2011; 39: 104–107.
24. Lu Q, Huang WQ, Wang Y, et al. Optimization design of deep-notch elliptical flexure hinges. *Opt Precis Eng* 2015; 23: 206–215.